Thioctic Acid–Functionalized Silica for Selective Palladium Adsorption from Chloride–based Solutions

Amir Nobahar[1*], Flavia N. Braga[1,2], Rita M. Carvalho[2,3], Helena Passos[2], Filipe H. B. Sosa[1], Nicolas Schaeffer[1*], João A. P. Coutinho[1]

[1]CICECO–Aveiro Institute of Materials, Department of Chemistry, University of Aveiro, 3810–193 Aveiro, Portugal

[2] LSRE–LCM, ALiCE, Faculty of Engineering, University of Porto, Rua Dr. Roberto Frias, 4200–465 Porto, Portugal.

[3] RYA – Purification Technologies, PCI – Creative Science Park, 3830–352 Ílhavo, Portugal

*Corresponding authors: anobahar@ua.pt, nicolas.schaeffer@ua.pt

Materials and methods

Materials

Silica gel 60 (0.2–0.5 mm) was purchased from Macherey-Nagel GmbH & Co. KG (Germany). DL-thioctic acid (α-lipoic acid, >98%) was obtained from Thermo Scientific. Hydrochloric acid (37%) was purchased from Fisher Scientific/Labsolve. Toluene (≥99.8%, HPLC grade), ethanol absolute (99.8%), dichloromethane (DCM, ≥99.8%), acetonitrile (≥99.8%, HPLC grade), and methanol (HPLC grade) were all obtained from Fisher Scientific. Ethanol (96%) was purchased from Carlo Erba. N,N'-dicyclohexylcarbodiimide (DCC, 99%) and (3-aminopropyl)trimethoxysilane (APTMS, 97%) were purchased from Sigma-Aldrich, while N-hydroxysuccinimide (NHS) (≥98%) was from Alfa Aesar. Molecular sieves 4 Å (8-12 mesh) were purchased from Acros Organics. Molecular sieves 3 Å (1-2 mm beads) were obtained from Alfa Aesar.

Standard metal solutions of 1000 $mg \cdot L^{-1}$ were purchased for Pt in 0.5 M HCl (BDH Chemicals Ltd, Poole, England) and Rh in 5% HCl (Sigma-Aldrich, Switzerland). Stock solutions of 1000 $mg \cdot L^{-1}$ of Pd, Fe, Zn and Ce, were prepared by dissolving proper quantities of analytical-grade reagents, including $PdCl_2$ (Sigma-Aldrich, USA), $FeCl_3$ (Thermo Fisher, Germany), $ZnCl_2$ (Thermo Scientific, USA), and $CeCl_3 \cdot 7H_2O$ (Merck, Germany), in deionized water.

Continuous-flow Fixed-Bed Column Studies

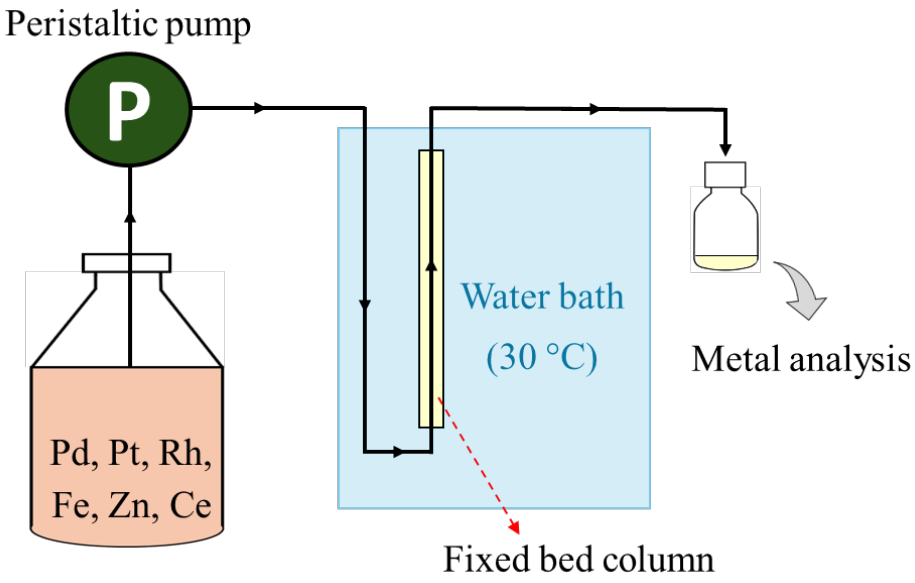

Figure S1. Schematic of the experimental setup used for continuous-flow fixed-bed column studies.

Characterization

The successful immobilization of TA on silica gel and the TA@Si before and after metal adsorption were characterized using a variety of analytical techniques. Raman spectroscopy was performed using a FT-RAMAN BRUKER MultiRAM spectrometer. The analysis utilized a Nd-YAG laser with a wavelength of 1064 nm and a power of 50 mW. The spectral resolution was set at 4 cm^{-1}, with 1000 scans collected over a range of 4000 to 50 cm^{-1}.

Fourier Transform Infrared (FTIR) spectra were recorded on a JASCO FT/IR-4X spectrometer equipped with a diffuse reflectance (DR PRO 410MX) accessory. Measurements were performed in the mid-infrared region (4000-350 cm^{-1}) with a spectral resolution of ~1 cm^{-1} in absorbance mode.

Solid-state carbon-13 cross-polarization magic-angle spinning nuclear magnetic resonance spectroscopy (^{13}C CP-MAS NMR) spectra were recorded on a Bruker Avance III 400 spectrometer operating at a magnetic field of 9.4 T, corresponding to a ^{13}C Larmor frequency of 100.6 MHz. Experiments were carried out using a double-resonance 4 mm

MAS probe under cross-polarization magic-angle spinning (CPMAS) conditions at a spinning speed of 12 kHz and ambient temperature. Samples were packed into zirconia rotors with Kel-F caps. ^{13}C chemical shifts are reported in ppm relative to α-glycine as a secondary reference (C=O at 176.50 ppm).

The morphology and elemental composition of TA@Si before and after the sorption process were evaluated using scanning electron microscopy coupled with energy-dispersive spectroscopy (SEM-EDS) on a HITACHI SU-70 apparatus operating at 25 kV, following carbon sputter-coating.

Scanning transmission electron microscopy (STEM) was performed on a Hitachi HD–2300 operated at 200 kV. Samples were dispersed in ethanol, sonicated for 5 min to break up agglomerates, and drop–cast onto carbon–coated copper grids. Imaging was conducted under slow–scan conditions (20 s per frame) with emission currents of 6–9 nA.

XPS spectra were acquired in an Ultra High Vacuum (UHV) system with a base pressure of 2×10^{-10} mbar located at TEMA, University of Aveiro. The system is equipped with a hemispherical electron energy analyzer (SPECS Phoibos 150), a delay-line detector and a monochromatic AlKα (1486.74 eV) X-ray source. High resolution spectra were recorded at normal emission take-off angle and with a pass-energy of 20 eV, which provides an overall instrumental peak broadening of 0.5 eV.

Thermogravimetric analysis coupled with differential scanning calorimetry (TG–DSC) was performed using a Setaram TG/DSC analyzer. Approximately 10 mg of dried sample was placed in the sample crucible and heated from room temperature to 800 °C at a heating rate of 10 °C·min^{-1} under N_2 atmosphere. For DSC evaluation, the heat-flow signal was recorded over the temperature range from room temperature to 300 °C under the same heating rate.

Nitrogen adsorption-desorption measurements were carried out at 77 K using a Micromeritics Gemini II surface area analyzer. The specific surface area was calculated by the Brunauer-Emmett-Teller (BET) method. The mesopore size distribution and total pore volume were determined using the Barrett-Joyner-Halenda (BJH) method, while t-plot analysis was employed to assess the presence of microporosity.

Elemental analysis was carried out to determine the carbon, hydrogen, nitrogen, and sulfur contents (expressed as weight percentages) using a Truspec Micro CHNS 630-200-200 elemental analyzer. Approximately 1 mg of sample was used for each measurement.

The combustion furnace was set to 1075 °C, and the afterburner operated at 850 °C. Carbon, hydrogen, and sulfur were quantified by infrared absorption, while nitrogen was measured using a thermal conductivity detector.

Concentration of Fe, Zn, Ce, Pd, Pt, and Rh were quantified using inductively coupled plasma-optical emission spectrometry (ICP-OES) on an iCAP 7400 system (Thermo Scientific), equipped with a nebulizing system and optical emission detection. Samples were diluted appropriately to ensure measurements fell within the calibration range (0.005-10 $mg \cdot L^{-1}$) and were analyzed in triplicate for accuracy.

Results and discussion

Structural and Spectroscopic Characterization of TA@Si

Table S1. CHNS elemental analysis of the Si-NH_2-TA.

Material	%C	%H	%N	%S
TA@Si	11.75 ± 0.16	2.23 ± 0.04	3.03 ± 0.03	2.41 ± 0.28

Table S2. Textural properties of silica before and after surface functionalization with APTMS and TA, determined from N_2 adsorption-desorption measurements at 77 K.

Sample	BET surface area, ($m^2 \cdot g^{-1}$)	Total pore volume ($cm^3 \cdot g^{-1}$)	Average pore diameter (nm)
Si	435.5 ± 0.4	0.724	6.65
Si–NH_2	250.7 ± 3.9	0.410	6.53
TA@Si	189.9 ± 1.1	0.265	5.57

Metal Adsorption Tests

Effect of HCl Concentration and Adsorption Kinetics

The separation factor (α) was calculated as follows:

$$\alpha_{Pd/Pt} = \frac{Kd_{Pd}}{Kd_{Pt}} \qquad \text{Eq. S1}$$

where Kd_{Pd} and Kd_{Pt} are the partition coefficients of Pd and Pt (L/g), respectively.

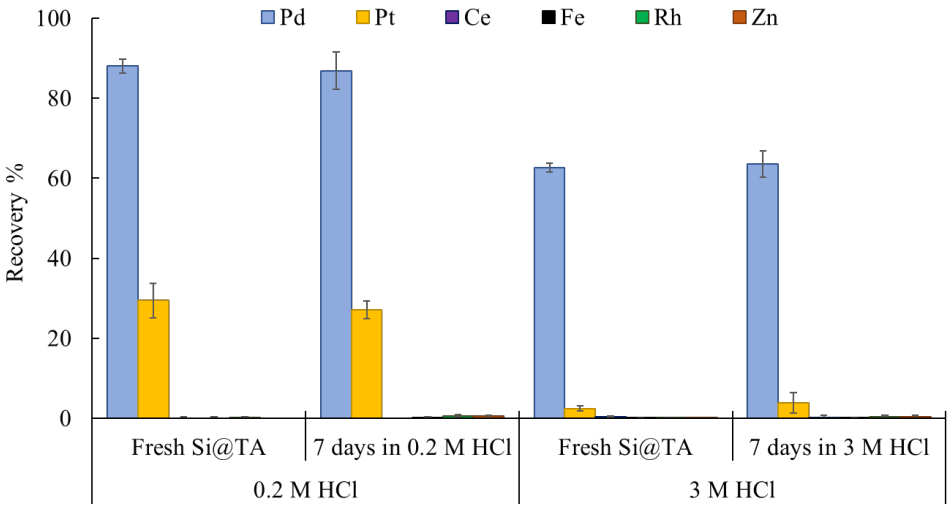

Figure S2. Metal adsorption performance of fresh TA@Si and pretreated TA@Si in 0.2 M and 3 M HCl under stirring for one week and subsequently used for metal adsorption from multi-metallic solutions prepared at the same respective HCl concentrations. Experimental conditions: TA@Si dosage of 1 $g \cdot L^{-1}$, multi-metallic solution containing (20 ± 2) $mg \cdot L^{-1}$ of each metal, temperature at 303 K, and contact time of 180 min.

Time-dependent adsorption experiments (up to 24 h) were conducted using TA@Si (1 $g \cdot L^{-1}$). To elucidate the adsorption mechanism, the kinetic profiles were modeled using nonlinear pseudo-first-order [1] (Eq. S2) and pseudo-second-order [2] (Eq. S3):

$$q_t = q_e(1 - e^{-k_1 t}) \qquad \text{Eq. S2}$$

$$q_t = \frac{q_e^2 \,.\, k_2 \,.\, t}{1 + q_e \,.\, k_2 \,.\, t} \qquad \text{Eq. S3}$$

In these models, q_t and q_e denote the sorption capacities ($mg \cdot g^{-1}$) at time t (min) and at equilibrium, respectively, while k_1 (min^{-1}) and k_2 ($g \cdot mg^{-1} \cdot min^{-1}$) represent the pseudo-first-order and pseudo-second-order rate constants.

Table S3. Kinetic parameters obtained from nonlinear pseudo-first-order and pseudo-second-order models for the adsorption of Pd and Pt onto TA@Si, along with their correlation coefficients (R^2).

Metal	$q_{e,exp}$ ($mg \cdot g^{-1}$)	Pseudo-first order model			Pseudo-second order model		
		$q_{e,cal}$ ($mg \cdot g^{-1}$)	R^2	k_1 (min^{-1})	$q_{e,cal}$ ($mg \cdot g^{-1}$)	R^2	k_2 ($g \cdot mg^{-1} \cdot min^{-1}$)
Pd	15.28 ± 0.24	14.19	0.71	0.08	15.20	0.96	0.01
Pt	2.37 ± 0.26	2.35	0.96	0.03	2.59	0.99	0.01

Isotherm studies

The equilibrium adsorption behavior was evaluated using the Langmuir, Freundlich, Temkin, and Sips isotherm models, expressed in their nonlinear forms as follows:
The Langmuir isotherm assumes monolayer adsorption on a homogeneous surface with a finite number of identical sites [3] and is given by:

$$q_e = \frac{q_{max}\ K_L\ C_e}{1 + K_L\ C_e} \qquad \text{Eq. S4}$$

Where q_e ($mg \cdot g^{-1}$) is the equilibrium adsorption capacity, C_e ($mg \cdot L^{-1}$) is the equilibrium concentration of the adsorbate, q_{max} ($mg \cdot g^{-1}$) represents the maximum monolayer adsorption capacity, and K_L ($L \cdot mg^{-1}$) is the Langmuir affinity constant.

The Freundlich isotherm describes adsorption on heterogeneous surfaces [4] and is expressed as:

$$q_e = K_F\ C_e^{1/n} \qquad \text{Eq. S5}$$

where K_F $((mg \cdot g^{-1})(L \cdot mg^{-1})^{1/n}$ is the Freundlich constant related to adsorption capacity, and n is the heterogeneity factor.

The Sips isotherm, which combines the Langmuir and Freundlich models to account for surface heterogeneity at low adsorbate concentrations and predicts monolayer adsorption at high concentrations [5], is given by:

$$q_e = \frac{q_{max}\ K_S\ C_e^n}{1 + K_S\ C_e^n} \qquad \text{Eq. S6}$$

Where K_S is the Sips equilibrium constant and n is the heterogeneity parameter. When n=1, the Sips model reduces to the Langmuir isotherm.

The Temkin isotherm accounts for adsorbate-adsorbent interactions and assumes that the heat of adsorption decreases linearly with surface coverage [6]:

$$q_e = \frac{RT}{b_T}\ln(K_T\, C_e) \qquad \text{Eq. S7}$$

where R (8.314 J·mol^{-1}·K^{-1}) is the universal gas constant, T (K) is the absolute temperature, b_T (J·mol^{-1}) is the Temkin constant related to the heat of adsorption, and K_T (L·mg^{-1}) is the Temkin equilibrium binding constant.

Table S4. Isotherm model parameters obtained from fitting experimental data of Pd and Pt adsorption onto TA@Si.

Model	Parameter	0.2 M HCl		3 M HCl	
		Pd	Pt	Pd	Pt
Langmuir	q_{max} (mg·g^{-1})	37.69	6.80	26.41	6.29
	K_L (L·mg^{-1})	0.10	0.05	0.13	0.00
	R^2	0.97	0.94	0.99	0.94
	R_L	0.89	0.85	0.87	0.97
Sips	q_{max} (mg·g^{-1})	49.51	7.06	29.02	2.06
	K_S (L·mg^{-1})	0.05	0.05	0.10	0.03
	n	0.72	0.80	0.83	2.59
	R^2	0.99	0.96	0.99	0.97
Temkin	K_T (L·g^{-1})	1.35	0.62	1.75	0.15
	b_T (kJ·mol^{-1})	0.33	1.78	0.48	3.67
	R^2	0.99	0.96	0.99	0.86
Freundlich	K_F (mg·g^{-1})(L·mg^{-1})$^{1/n}$	6.65	1.01	6.09	0.05
	n	2.46	2.54	2.93	1.19
	R^2	0.97	0.95	0.95	0.93

Adsorption mechanism

Thermodynamics

The thermodynamics of metal adsorption onto TA@Si were investigated by measuring adsorption efficiencies in 0.2 and 3 M HCl at 303, 313, 323, and 333 K. As shown in Figure 5–A and B, increasing the temperature enhanced the adsorption capacities of Pd

and Pt at both acid concentrations. In contrast, adsorption of the base metals (Ce, Fe, Zn) remained negligible, while only a slight increase was observed for Rh.

To evaluate the feasibility and thermodynamic nature of the adsorption process, key parameters including the enthalpy change (ΔH, J·mol^{-1}), entropy change (ΔS, J·mol^{-1}), and Gibbs free energy change (ΔG, J·mol^{-1}) were determined. These parameters were obtained using the Van't Hoff relationship (Eq. S8):

$$lnK = -\frac{\Delta H}{RT} + \frac{\Delta S}{R} \qquad \text{Eq. S 8}$$

where K is the dimensionless thermodynamic equilibrium constant, T is the absolute temperature (K), and R is the universal gas constant (8.314 J·mol^{-1}·K^{-1}). The equilibrium constant was initially estimated from the distribution coefficient (K_d, L·g^{-1}), defined as:

$$K_d = \frac{q_e}{C_e} \qquad \text{Eq. S9}$$

where q_e (mg·g^{-1}) is the equilibrium adsorption capacity and C_e (mg·L^{-1}) is the equilibrium concentration of the solute. However, the direct use of K_d as a thermodynamic constant is inappropriate due to its dimensional nature and limited physical meaning, as highlighted by Tran [7]. Therefore, a dimensionless equilibrium constant (K) was obtained by normalizing K_d with the standard adsorbent concentration (1 g·L^{-1}):

$$K = K_d \times adsorbent\ dose\ (\text{g·L}^{-1}) \qquad \text{Eq. S10}$$

The Gibbs free energy change was then calculated as:

$$\Delta G = -RTlnK \qquad \text{Eq. S11}$$

Spectroscopic analyses

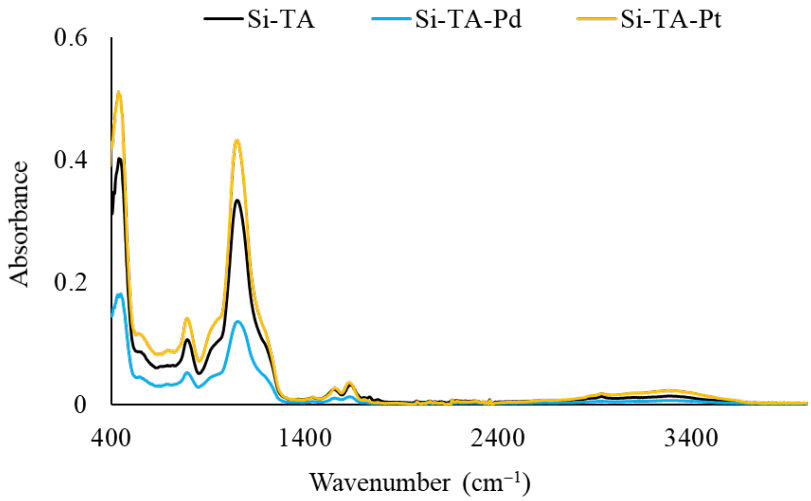

Figure S3. FTIR spectra of TA@Si, before and after Pd or Pt adsorption. Experimental conditions: TA@Si dosage of 1 $g \cdot L^{-1}$, single-metal solutions of (100 ± 5) $mg \cdot L^{-1}$ in 0.2 M HCl, contact time of 180 min, and temperature at 303 K.

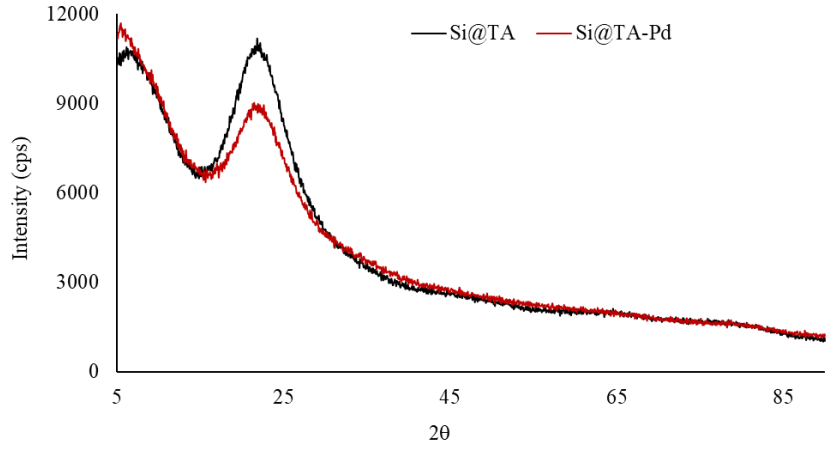

Figure S4. XRD spectra of TA@Si before and after Pd adsorption. Experimental conditions: TA@Si dosage of 1 $g \cdot L^{-1}$, single-metal solutions of (100 ± 5) $mg \cdot L^{-1}$ in 0.2 M HCl, contact time of 180 min, and temperature at 303 K.

Table S5. Normalized elemental abundances of TA@Si after Pd adsorption from 100 $mg \cdot L^{-1}$ synthetic solution in 0.2 M HCl, determined by SEM-EDS from the area in Figure 6–B.

Element	[norm. wt.%]	[norm. at.%]
O	69.92	77.22

C	11.51	16.93
Pd	10.78	1.79
Cl	4.41	2.20
S	3.38	1.86
Total	100	100

Table S6. Binding energy and relative abundance % of TA@Si before and after Pd adsorption. Experimental conditions: TA@Si dosage of 1 $g \cdot L^{-1}$, single–metal solutions of (100 ± 5) $mg \cdot L^{-1}$ in 0.2 M HCl, contact time of 180 min, and temperature at 303 K.

	TA@Si		**TA@Si + Pd**		**Correlated groups**
	BE	**RA**	**BE**	**RA**	
C 1s	285.34	50.4	286.24	23.6	C–S, C–N, C–O
	284.80	34.0	284.80	36.3	C–C, C–H
	288.47	4.4	287.75	20.6	C=O, C–N–C
O 1s	529.58	14.1	531.07	68.0	C=O, carboxylate oxygen
	532.44	85.9	533.01	32.0	Si–O–Si, O–C=O
N 1s	402.77	82.5	403.10	76.0	C–N–C, N–C
	400.01	5.3	401.02	16.8	$C–NH_2$
	397.25	12.2	397.47	7.2	
S 2p	164.15	43.2	164.88	45.5	S–S
	165.38	34.5	166.14	34.9	
	160.95	13.7	162.41	12.8	–SH, S–Pd
	162.07	8.6	163.55	6.8	
Pd 3d	–	–	338.25	56.6	Pd^{2+}
			343.60	43.4	
Cl 2p	–	–	198.42	61.4	Cl^-
	–	–	200.23	38.6	

Batch Adsorption-Desorption Studies

The desorption efficiency (D%) of each metal was then calculated as the percentage of the total adsorbed metal released into solution by each desorption agent, using the Equation S1:

$$D(\%) = \frac{C_d V_d}{q_{ads} m} \times 100 \qquad \text{Eq. S12}$$

where C_d (mg·L^{-1}) is the concentration of metal in the desorption solution, V_d (L) is the volume of the desorption solution, q_{ads} (mg·g^{-1}) is the amount of metal previously adsorbed on the adsorbent, and m (g) is the mass of the adsorbent used.

Continuous-flow fixed-bed column studies

Breakthrough curves for the adsorption of PGMs onto TA@Si in a fixed-bed column using a multimetallic solution containing (50 ± 5) mg·L^{-1} of each metal in 0.2 M HCl (flow rate: 1 mL·min^{-1}; bed mass: 0.5435 g; bed radius: 0.25 cm; bed height: 4 cm; temperature: 303 K). The Pd breakthrough profile was successfully fitted using Thomas, Bohart–Adams, and Yoon–Nelson models. In contrast, Pt, Rh, and the remaining metals exhibited either immediate breakthrough or negligible adsorption, with C_t/C_0 values remaining close to unity throughout the experiment, preventing reliable parameter estimation and model fitting.

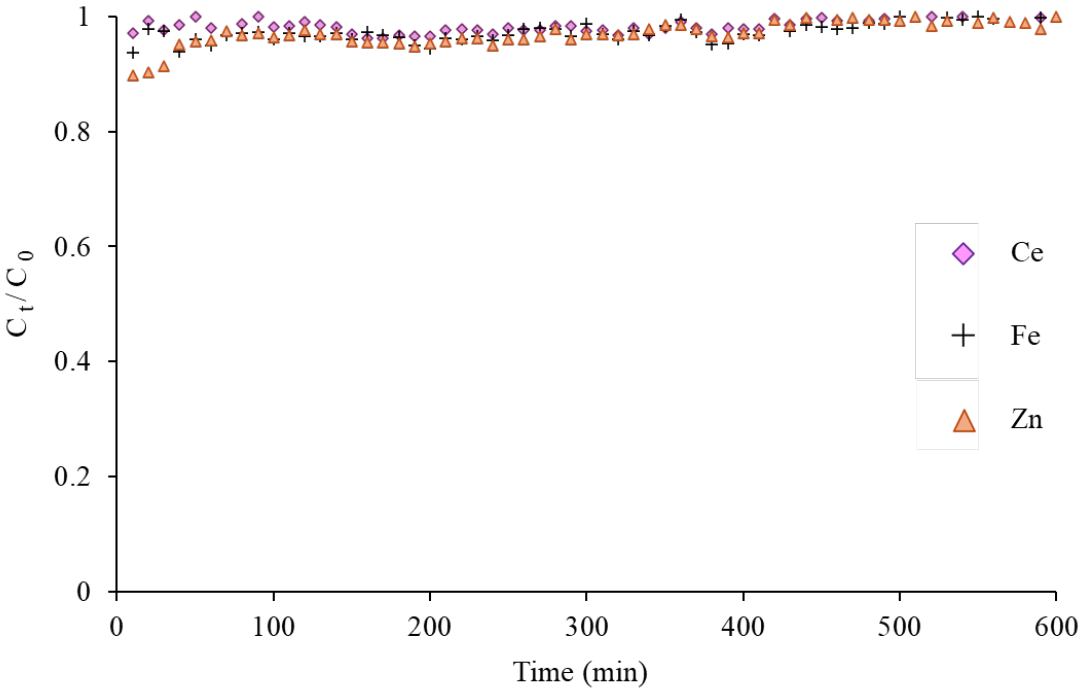

Figure S5. Breakthrough curves for the adsorption of non-PGMs onto TA@Si in a fixed-bed column. Experimental conditions: multi-metallic solution containing (50 ± 5) $mg \cdot L^{-1}$ of each metal in 0.2 M HCl, flow rate of 1 $mL \cdot min^{-1}$, bed mass = 0.5435 g, bed radius = 0.25 and height = 4 cm (bed volume ≈ 0.785 cm^3), temperature at 303 K.

Table S7. Breakthrough characteristics and adsorption capacities for Pd, Pt, and Rh adsorption onto TA@Si in fixed-bed column experiments. Model-fitting parameters obtained from the Thomas, Bohart-Adams, and Yoon–Nelson models are reported for Pd only. Experimental conditions are given in Figure 8.

Parameter		Unit	Pd	Pt	Rh
Breakthrough time, t_a (C_t/C_0 = 0.05) (min)		min	195	14	–
Bed volumes processed at breakthrough		BV	248.41	18	–
Dynamic breakthrough capacity (q_{dyn} at C_t/C_0 = 0.05)		$mg \cdot g^{-1}$	18.10	1.70	–
Exhaustion time (C_t/C_0 = 0.90)		min	580	110	40
Total dynamic capacity (q_{total})		$mg \cdot g^{-1}$	34.14	4.44	0.51
Thomas model	Rate constant (k_{Th})	$mL \cdot mg^{-1} \cdot min^{-1}$	2.15×10^{-5}	–	–
	Thomas maximum adsorption capacity (q_{Th})	$mg \cdot g^{-1}$	36.70	–	–
	Correlation coefficient (R^2)	–	0.99	–	–
Bohart-Adams model	Rate constant (k_{BA})	$L \cdot mg^{-1} \cdot min^{-1}$	3.19×10^{-4}	–	–
	Saturation concentration (N_0)	$mg \cdot L^{-1}$	2.19×10^{4}	–	–
	Correlation coefficient (R^2)	–	0.88	–	–
Yoon–Nelson model	Rate constant (k_{YN})	min^{-1}	0.01	–	–
	Time for 50% breakthrough (τ)	min	376.38	–	–
	Correlation coefficient (R^2)	–	0.99	–	–

References

[1] S. Lagergren, Zur Theorie der sogenannten Adsorption gelöster Stoffe, Bihang till Kungliga Svenska Vetenskapsakademiens Handlingar 24 (1898) 1–39.

[2] Y.S. Ho, G. McKay, Pseudo-second order model for sorption processes, Process Biochem. 34 (1999) 451–465. https://doi.org/10.1016/S0032-9592(98)00112-5.

[3] I. Langmuir, THE CONSTITUTION AND FUNDAMENTAL PROPERTIES OF SOLIDS AND LIQUIDS. PART I. SOLIDS., J. Am. Chem. Soc. 38 (1916) 2221–2295. https://doi.org/10.1021/ja02268a002.

[4] H. Freundlich, Über die Adsorption in Lösungen, Z. Für Phys. Chem. 57U (1907) 385–470. https://doi.org/10.1515/zpch-1907-5723.

[5] R. Sips, On the Structure of a Catalyst Surface, J. Chem. Phys. 16 (1948) 490–495. https://doi.org/10.1063/1.1746922.

[6] M. Temkin, V. Pyzhev, Kinetics of Ammonia Synthesis on Promoted Iron Catalysts, Acta Physicochimica U.R.S.S. 12 (1940) 327–356.

[7] H.N. Tran, Improper Estimation of Thermodynamic Parameters in Adsorption Studies with Distribution Coefficient K_D (q_e/C_e) or Freundlich Constant (K_F): Considerations from the Derivation of Dimensionless Thermodynamic Equilibrium Constant and Suggestions, Adsorpt. Sci. Technol. 2022 (2022). https://doi.org/10.1155/2022/5553212.